Large-shift Raman scattering in insulating parent compounds of cuprate superconductors

D. Salamon,* Ran Liu,† M. V. Klein, M. A. Karlow, and S. L. Cooper
Science and Technology Center for Superconductivity, Department of Physics, and Materials Research Laboratory, University of Illinois at Urbana-Champaign, 104 S. Goodwin Ave., Urbana, Illinois 61801

S-W. Cheong
AT&T Bell Laboratories, Murray Hill, New Jersey 07974

W. C. Lee‡ and D. M. Ginsberg
Science and Technology Center for Superconductivity, Department of Physics, and Materials Research Laboratory, University of Illinois at Urbana-Champaign, 104 S. Goodwin Ave., Urbana, Illinois 61801

(Received 19 July 1994)

We describe the use of large-shift Raman techniques to probe features near the optical conductivity peak in insulating high-T_c parent compounds, including the T'-phase materials (R_2CuO_4, R=Gd, Eu, Sm, Nd, Pr), T-phase La_2CuO_4, and 123-phase $PrBa_2Cu_3O_6$ and $YBa_2Cu_3O_6$. We have observed several features near 12 000 cm^{-1} ($\sim$1.5 eV) with A_{2g}, B_{1g}, and A_{1g} symmetry. At low temperatures, the largest feature with A_{2g} symmetry splits in all the insulating cuprates into three distinct peaks: a strong main peak, and two weaker sidebands offset approximately 600 and 1500 cm^{-1} higher in energy, respectively. A B_{1g} feature coinciding in position with the optical conductivity peak is observed in all the T' phase materials, but not in the other insulators. An A_{1g} peak is observed in Gd_2CuO_4 and Eu_2CuO_4 40–50 cm^{-1} lower in energy than the main A_{2g} peak, and in $YBa_2Cu_3O_6$ around 2400 cm^{-1} above the main A_{2g} peak. All of these features have unusual, temperature-dependent resonance behavior with the incident photon energy. We propose explanations for many of the above observations involving copper $d_{x^2-y^2}$ to d_{xy} hole transitions enabled by coupling to oxygen p_σ and p_π levels.

I. INTRODUCTION

Much of recent research on high-temperature superconductors has focused on the role of the copper-oxygen planes in the superconducting properties. Accurate studies of these materials are often complicated, however, by sample-preparation difficulties as well as inaccurate determinations of the in-plane carrier concentrations. By instead studying the insulating parent compounds of the high-temperature superconductors, we can avoid many of these problems and isolate the properties of the copper-oxygen planes from any effects of the apical oxygens. Further, we can examine the magnetic properties of these materials without additional complications from in-plane carriers.

Even with their somewhat simpler structure, however, the properties of the insulating parent compounds are not well understood. The cuprate insulators seem to behave as charge-transfer insulators,[1] with a "charge-transfer gap" around 1.7–2 eV as measured by infrared reflectivity.[2–4] High-energy spectroscopic studies suggest that the lowest unoccupied states near the edge of the gap are hybrids, with largely copper $d_{x^2-y^2}$ and some oxygen p_σ character.[5–8] Neutron-diffraction experiments have revealed long-range antiferromagnetic ordering with Néel temperatures in the range 250–500 K.[9–12] Magnon excitations in this ordered state have been measured by both Raman[13–16] and neutron-diffraction[10,17] techniques. Resonant Raman experiments have also shown that the intermediate states participating in these magnetic fluctuations are not simple charge transfers.[18,19]

In order to probe both the symmetry of states near the charge-transfer gap and the nature of the intermediate states involved in magnetic fluctuations, we recently demonstrated for the first time the technique of large-shift Raman scattering.[18–21] Using this method, we discovered a Stokes feature in several of the cuprate insulators near 12 000-cm^{-1} (1.5 eV) Raman shift at room temperature.[18,20,21] We also established that this feature had unusual A_{2g} or pseudovector symmetry.[18,20,21] Note that Wake[22] has recently observed a similar feature in $YBa_2Cu_3O_6$. He did not, however, perform any symmetry analysis of his peak, and the resonance behavior he observes differs in important ways from our results.

Here we present the first systematic large-shift Raman study of the cuprate insulators, including T'-phase (R_2CuO_4, R=Gd, Eu, Sm, Nd, Pr), T-phase (La_2CuO_4), and 123-phase ($RBa_2Cu_3O_6$, R=Y, Pr) materials. Additional doping-dependence results from $YBa_2Cu_3O_{6+x}$ will be published separately.[23] This variety of insulating materials brings out several trends involving copper-oxygen bond length and oxygen coordination number. Additional temperature-dependence and resonant Raman studies allow us to identify a number of common characteristics across all of the cuprate insulators, and finally to propose a possible model to explain some of the Raman features.

II. DESCRIPTION OF THE EXPERIMENT

For this study, we employed both the pseudo- and true-backscattering configurations. Polarization geometries are described using the Porto notation $i(jk)l$, where i,l represent the propagation directions and j,k the polarizations of the incident and scattered light, respectively. All directions are in terms of the sample axes, with the optical x, y, and z directions parallel to the crystal axes a, b, and c. The additional x' and y' optical directions are rotated 45° counterclockwise in-plane with respect to the crystal axes a and b.

Laser excitation in this study involved ultraviolet (UV) light at 325.0 nm (3.81 eV) from a HeCd laser, and at 333.6 nm (3.72 eV), 334.5 nm (3.71 eV), 351.1 nm (3.53 eV), and 363.8 nm (3.41 eV) from an argon laser. We employed an external 60° prism to split the argon laser UV lines, orienting both the prism and the laser polarization into a Brewster configuration to maximize UV throughput. Typical laser power levels at the sample were around 9–10 mW for the 333.6- and 334.5-nm lines, and 15–20 mW for the 351.1- and 363.8-nm lines. In order to eliminate laser plasma luminescence, we used both diaphragm apertures and a UV-transmitting–visible-blocking colored-glass filter.

The detection apparatus consisted of a SPEX Triplemate spectrometer with 150 groove-mm grating in all three stages and a Photometrics 512 pixel×512 pixel CCD array detector. Even with these gratings, the wide spectral range used in this study required that a total of five different CCD "windows" be linked together. These windows were centered at 400.0, 490.0, 580.0, 670.0, and 760.0 nm and covered approximately 900 nm (or 2300 cm^{-1}) each. We accounted for chromatic aberration in the collection optics by underfilling the 300-μm spectrometer entrance slit with our laser spot and using "binning" to combine many CCD pixels into one unit. The laser spot was approximately 100 μm in diameter, providing a resolution of around 20–30 cm^{-1}. In most cases, however, the actual resolution depended more on the signal-to-noise level and breadth of the observed features.

The raw data taken from the CCD detector were corrected in several ways before arriving at the final form used for this article, i.e., normalized data directly proportional to the photon scattering cross section $d\sigma/d\omega$. First, after subtracting away an averaged dark count from the raw data, we corrected for the nonlinear spectral response of our detection system by employing a LabSphere standardized lamp. The calibration data were additionally smoothed to improve the signal-to-noise ratio. Second, we divided our data by a factor of ω^2 (with ω in absolute cm^{-1}) to arrive at corrected data proportional to a photon cross section. This was necessary to convert from CCD pixels measuring a wavelength range $\Delta\lambda$ to data points measuring a wave number range $\Delta\omega$.

Finally, in order to compare results taken with different laser wavelengths, all data were normalized to the same incident laser power of 10 mW at 333.6 nm, corresponding to a power density of approximately 4 MW/m^2. Data taken at low temperatures in our cryostat were also normalized for the wavelength-dependent transmission coefficients of the Dewar windows. We did not, however, correct for any sample-specific absorption, transmission, or refraction effects since the optical constants in these materials do not change appreciably over the visible and UV energy ranges.[24,25] Note that in all of the sections to follow, the data are offset for clarity in plots involving multiple spectra.

The T- and T'-phase single-crystal samples used in this study included La_2CuO_4, Gd_2CuO_4, Eu_2CuO_4, Sm_2CuO_4, Nd_2CuO_4, and Pr_2CuO_4. All were prepared using techniques described previously,[26,27] involving a CuO- and PbO-based flux method in a platinum crucible. Most of the crystals used in this study were platelike parallelepipeds roughly 2–3 mm on a side, with thicknesses around 0.1 mm. The Sm_2CuO_4 crystal was about 0.5 cm×0.5 cm in size, although some of this area had facets and was unsuitable for Raman scattering. The La_2CuO_4 sample also was very large, around 1 cm×1 cm, but the entire surface was faceted.

The 123-phase single crystals used in this study included $PrBa_2Cu_3O_6$ and $YBa_2Cu_3O_{6.1}$. Both were prepared using techniques published previously,[28,29] involving a

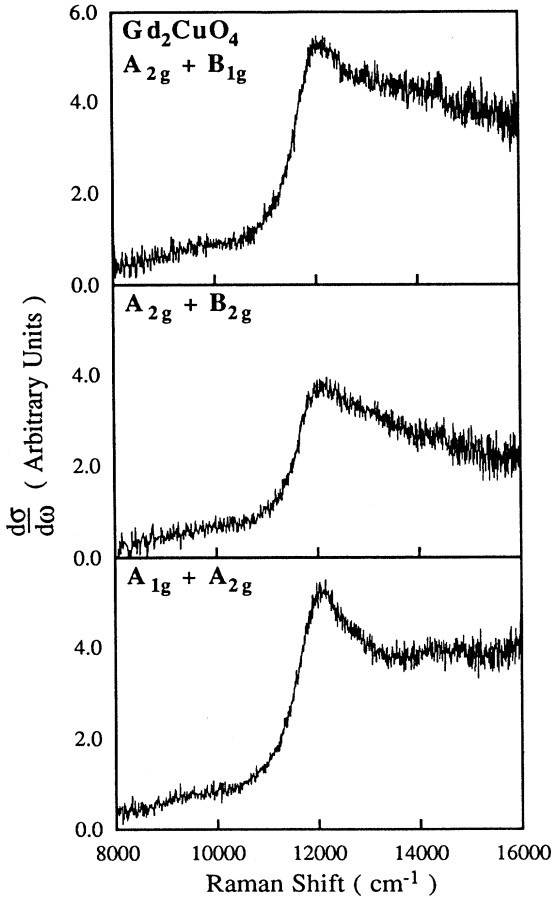

FIG. 1. Raman data on Gd_2CuO_4 at room temperature with the laser at 325.0 nm. The true-backscattering geometries are $z(x'y')\bar{z}$ ($A_{2g}+B_{1g}$), $z(xy)\bar{z}$ ($A_{2g}+B_{2g}$), and $z(x+iy,x+iy)\bar{z}$ ($A_{1g}+A_{2g}$).

CuO flux method in a yttria-stabilized zirconia crucible. To reduce the oxygen content, the crystals were further annealed in nitrogen gas. Both of the 123-phase crystals were platelike parallelepipeds, around 1–2 mm on a side. Their thickness was around 50–100 μm.

The crystal axis orientations for all of the above samples were measured using Laue x-ray diffraction. Surface contamination proved an important problem in this study since the resulting luminescence tended to overwhelm the Raman signal. We therefore ensured as much as possible that all samples had mirrorlike surfaces by carefully cleaning them with high-purity methanol. Additionally, some of our $YBa_2Cu_3O_6$ samples were etched in a solution consisting of 1% bromine and 99% methanol to confirm that our observations were not parasitic surface effects.

III. RAMAN-SCATTERING RESULTS

A. T'-phase materials

We begin by examining the symmetry of our scattering features at room temperature, where it was possible for us to use the true-backscattering configuration and circular polarization geometry. Figures 1 and 2 show a symmetry analysis on Gd_2CuO_4, which is similar in most respects to the results from the other materials we studied. There is a clearly defined peak in Fig. 1 near 12 000 cm^{-1} with A_{2g} or pseudovector symmetry. Two additional features are also clear in Fig. 2, a broad one with B_{1g} symmetry near 13 000 cm^{-1}, and one with A_{1g} symmetry near 11 900 cm^{-1}. There seem to be no features with B_{2g} symmetry. The barely resolved bump near 12 000 cm^{-1} in the $B_{1g}+B_{2g}$ spectrum of Fig. 2 is likely a small amount of leakage due to a slightly misaligned $\lambda/4$ plate.

Figure 3 shows room-temperature data in the $A_{2g}+B_{2g}$ scattering geometry for all of the T' series, plotted along with the corresponding optical conductivity curve. There is a clear trend in which the A_{2g} peak shifts position through the series to remain approximately 1600 cm^{-1} below the peak in the optical conductivity spec-

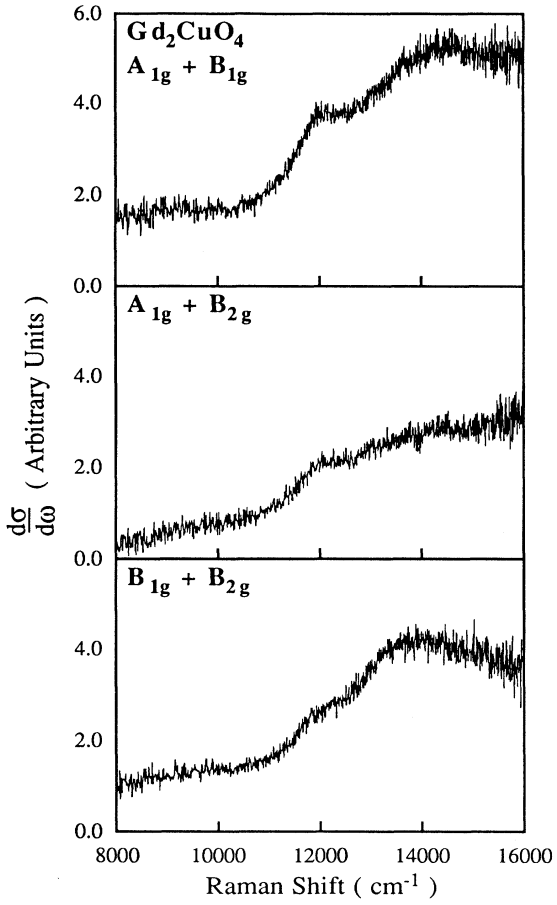

FIG. 2. Raman data on Gd_2CuO_4 at room temperature with the laser at 325.0 nm. The true-backscattering geometries are $z(xx)\bar{z}$ ($A_{1g}+B_{1g}$), $z(x'x')\bar{z}$ ($A_{1g}+B_{2g}$), and $z(x+iy,x-iy)\bar{z}$ ($B_{1g}+B_{2g}$).

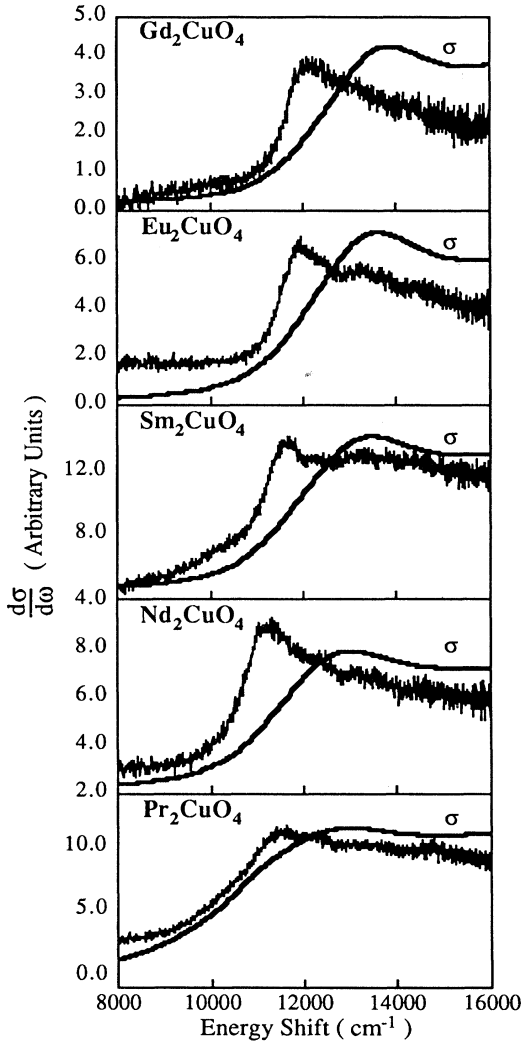

FIG. 3. Raman data on the T' series at room temperature in the $z(xy)\bar{z}$ ($A_{2g}+B_{2g}$) true-backscattering geometry with the laser at 325.0 nm. Also plotted on a different scale is the optical conductivity σ for each material.

trum. Such behavior points toward an excitonic origin, although excitons ordinarily have E_u (dipole) rather than A_{2g} symmetry. The energy difference of 1600 cm^{-1} ($\sim$0.2 eV) is, however, close to twice the exchange parameter J,[14] and may also match the energy difference between some of the p-d hybridized orbitals in the copper-oxygen bonds.

In Fig. 4, we show the $B_{1g}+B_{2g}$ spectrum, as well as the optical conductivity, at room temperature for all of the T' series. As we have observed no B_{2g} features, Fig. 4 shows pure B_{1g} scattering. Again, a trend is clear in which the broad B_{1g} peak seems to align almost exactly with the peak in the optical conductivity spectrum for all the T' materials. Now, electronic absorption in optical conductivity spectra is largely electric-dipole in nature with E_u symmetry. It thus seems likely that the B_{1g} peak is actually Raman-forbidden scattering by the same E_u states producing the peak in the optical conductivity.

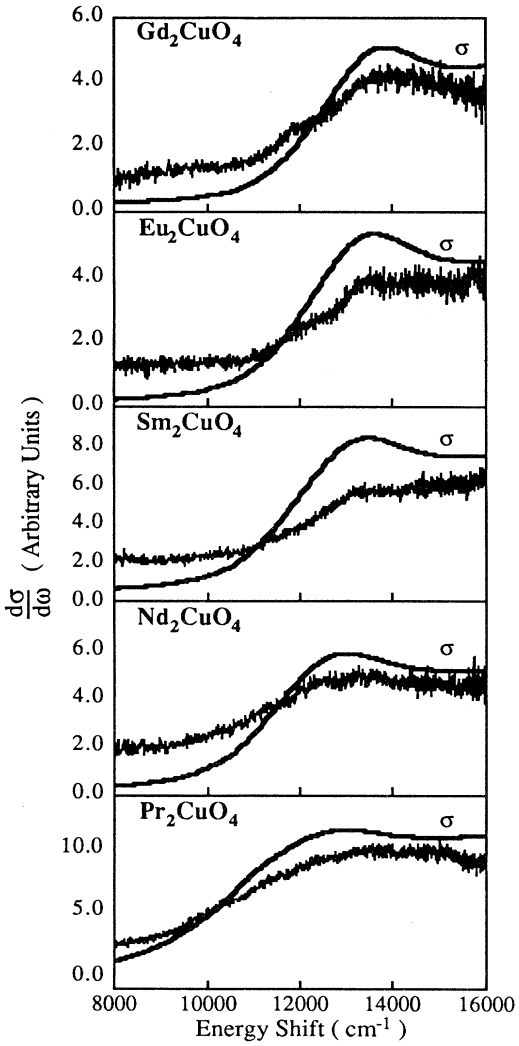

FIG. 4. Raman data on the T' series at room temperature in the $z(x+iy,x-iy)\bar{z}$ ($B_{1g}+B_{2g}$) true-backscattering geometry with the laser at 325.0 nm. Also plotted on a different scale is the optical conductivity σ for each material.

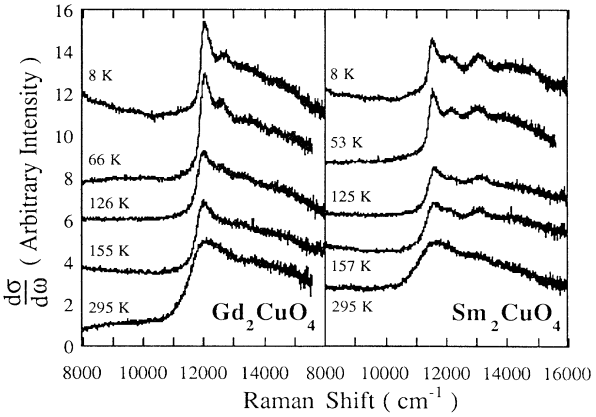

FIG. 5. Temperature dependence of the A_{2g} Raman features in the $z(xy)\bar{z}$ ($A_{2g}+B_{2g}$) pseudobackscattering geometry with the laser at 333.6 nm. Data are shown for both Gd_2CuO_4 and Sm_2CuO_4.

Such behavior can arise from strong electron-phonon or electron-magnon coupling, although these phenomena are usually observed in the context of phonon Raman scattering.[30–32]

The temperature dependence of the A_{2g} peak is particularly interesting, as shown in Fig. 5 for both Gd_2CuO_4 and Sm_2CuO_4. The single A_{2g} feature at 295 K is seen to split into three distinct peaks, all with the same A_{2g} symmetry. The strongest of these is the one with the lowest scattering energy, followed by two additional "sidebands" with lower amplitude. Although there seems to be no shift with temperature in the position of the strongest peak, its separation from the optical conductivity peak changes to be around 2150 cm^{-1} at low temperatures as a result of displacement in the optical conductivity peak position (see Fig. 7). The splitting between the strongest peak and the first sideband is approximately 600 cm^{-1}, and between the first sideband and the second

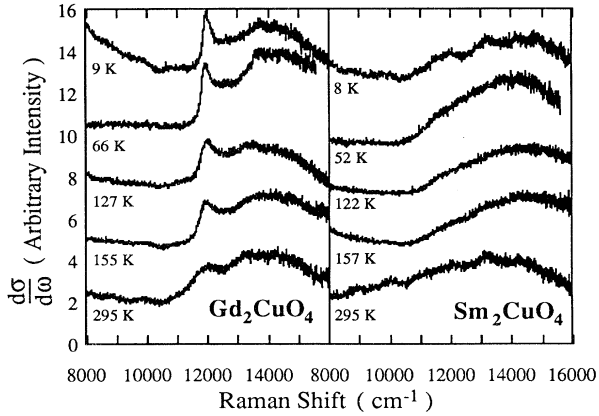

FIG. 6. Temperature dependence of the B_{1g} and A_{1g} Raman features in the $z(xx)\bar{z}$ ($A_{1g}+B_{1g}$) pseudobackscattering geometry with the laser at 333.6 nm. Data are shown for both Gd_2CuO_4 and Sm_2CuO_4.

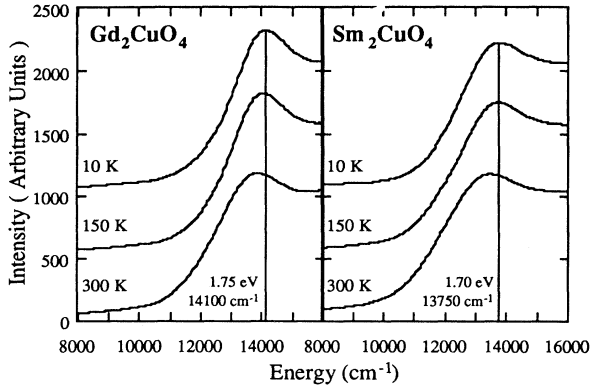

FIG. 7. Temperature dependence of the optical conductivity in Gd_2CuO_4 and Sm_2CuO_4 near the charge-transfer gap. A vertical line is drawn to illustrate the shift in position of the main peak.

sideband approximately 850 cm^{-1}. All of the above behavior has been observed throughout the T' series, although the sidebands are somewhat difficult to identify in the case of Pr_2CuO_4 (see Fig. 9).

Figure 6 shows the temperature dependence of the B_{1g} and A_{1g} features in Gd_2CuO_4 and Sm_2CuO_4. The A_{1g} peak in Gd_2CuO_4 gets noticeably sharper at lower temperatures, but does not seem to shift in position. In fact, it is only at low temperatures that it is possible to really see the difference in position between the A_{1g} and A_{2g} peaks. We will discuss the A_{1g} peak in more detail below in the context of resonant behavior. The B_{1g} feature is interesting because it seems to be the only one of these Raman peaks that shifts with temperature. This shift of around 500 cm^{-1} toward higher energies seems to occur between room temperature and 150 K for both Gd_2CuO_4 and Sm_2CuO_4, as shown in Fig. 6. Interestingly, the shift in the B_{1g} feature seems to match the shift with temperature in the optical conductivity peak position. As Fig. 7 shows, the optical conductivity shift also occurs between room temperature and 150 K, and is also around 500 cm^{-1} toward higher energies. Thus, the B_{1g} feature tracks the optical conductivity peak with temperature. Such evidence tends to support the idea that the B_{1g} Raman feature is actually Raman-activated E_u scattering at the charge-transfer gap edge, although the activation mechanism is unclear.

All of the large-shift Raman features seem to also show unusual temperature-dependent resonant behavior. Figure 8 shows A_{2g} resonance profiles for Gd_2CuO_4 at three different temperatures, illustrating several important trends. First, at 295 K it seems that all of the A_{2g} peaks resonate weakly toward photon energies higher than the available 3.72-eV line. The behavior of the high-energy portion of the peak, which contains the two unresolved sidebands, seems to indicate that the sidebands resonate slightly more strongly than the first peak. Then at 156 K there is little or no resonant behavior of the first peak, while the first sideband seems to resonate close to the 3.53-eV line, and the second sideband continues to resonate weakly for photon energies higher than 3.72 eV. Finally, at 8.5 K there is a dramatic resonant enhancement of the first peak for the redder 3.41-eV line, the first sideband seems to resonate somewhere between the 3.53- and 3.41-eV lines, and the second sideband again resonates weakly for photon energies higher than 3.72 eV.

All of this resonant behavior holds throughout the T' series, but it gets progressively weaker with increasing copper-oxygen bond length until there is almost no resonant behavior seen in Pr_2CuO_4, as shown in Fig. 9. Figure 9 also shows arrows pointing out the best-guess positions of the three A_{2g} "peaks" in Pr_2CuO_4 at 5.6 K. The large peak in the 3.53-eV spectrum of Pr_2CuO_4 is of unknown origin. It is not observed at room temperature, but does appear to be polarized. Now, Pr_2CuO_4 is known to be a somewhat disordered material in which some of

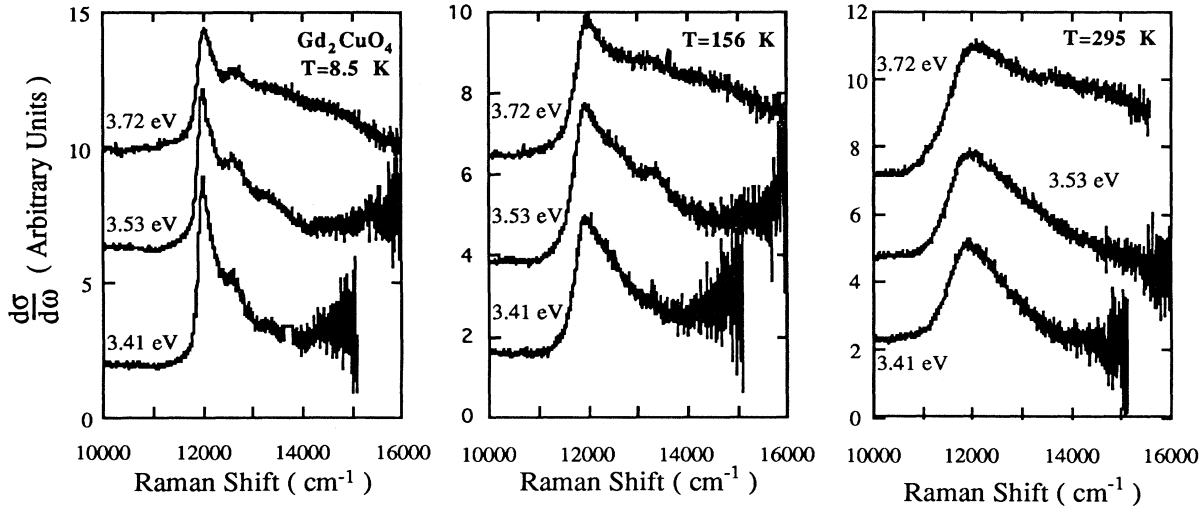

FIG. 8. Resonance behavior at three different temperatures for Gd_2CuO_4 in the $z(xy)\bar{z}$ ($A_{2g}+B_{2g}$) pseudobackscattering geometry. Laser energies are indicated in eV.

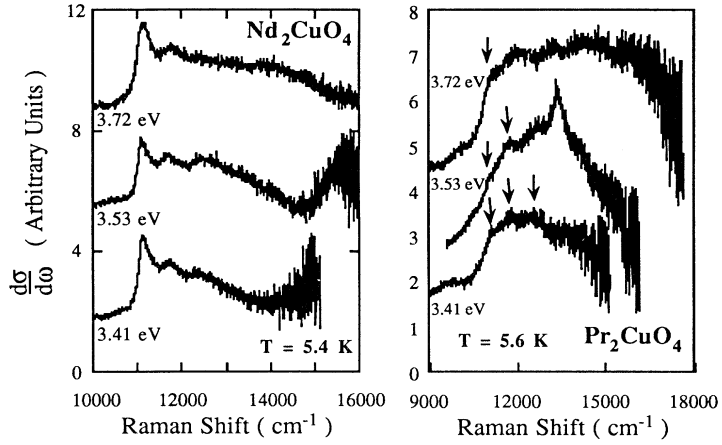

FIG. 9. Resonance behavior at low temperature for Nd_2CuO_4 and Pr_2CuO_4 in the $z(xy)\bar{z}$ ($A_{2g}+B_{2g}$) pseudobackscattering geometry. Laser energies are indicated in eV. Arrows indicate the main A_{2g} peak and sidebands in Pr_2CuO_4.

the O(2) atoms take up T-phase apical positions because of the oversized Pr ionic radius. Such disorder can produce many unusual symmetry-forbidden scattering effects, leading to behavior that is nontypical for T' materials.[33,34] Results from Pr_2CuO_4 are thus shown here mainly for confirmation purposes.

The resonant behavior of the B_{1g} and A_{1g} features is less dramatic than that of the A_{2g} peaks, and there is little temperature dependence. As shown in Fig. 10, the B_{1g} feature consistently resonates toward photon energies higher than 3.72 eV. This behavior holds through the T' series, but the resonance gets progressively weaker with increasing copper-oxygen bond length. Figure 10 also illustrates the presence of a strong A_{1g} peak in Gd_2CuO_4 and a weaker one in Eu_2CuO_4. The Gd_2CuO_4 A_{1g} peak is shifted 50 cm^{-1} below its A_{2g} peak (see Fig. 11), while the Eu_2CuO_4 A_{1g} peak is shifted 40 cm^{-1} below its A_{2g} peak. in both materials the A_{1g} peak seems to slightly resonate toward the 3.41-eV photon energy.

As seen in Fig. 6, the A_{1g} feature is not present in Sm_2CuO_4, nor in any other of the T' series. This behavior points strongly toward the known lattice distortion found in Gd_2CuO_4 and to a lesser extent in Eu_2CuO_4, involving a slight in-plane bending of the O(1) atoms. Evidence for such distortion comes from oversized x-ray thermal factors,[35] forbidden Raman phonon modes,[36,37] and observations of weak ferromagnetism.[38–41] This in-plane lattice distortion would seem to be breaking the symmetry of the main A_{2g} excitation, causing a splitting of around 50 cm^{-1} into two states with different symmetry. Such a phenomenon points strongly toward a localized copper excitation as the origin of the main A_{2g} peak.

B. T-phase materials

La_2CuO_4 presents a difficulty for the large-shift Raman technique employed in this work because the peak in its optical conductivity is near 2 eV, a higher energy than in the T' materials.[24] This means that features appearing near the charge-transfer gap in La_2CuO_4 come very close to the infrared limit of our detection equipment, even for the shortest-wavelength laser lines. As a result, in most cases it was not possible to use the 363.8-nm (3.41-eV) line, and data is very limited with the 351.1-nm (3.53-eV)

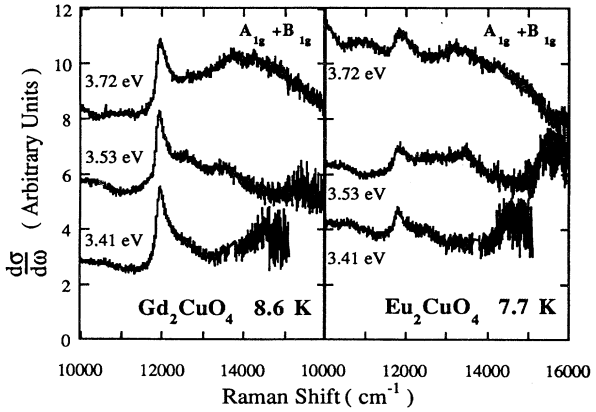

FIG. 10. Resonance behavior at low temperatures for Gd_2CuO_4 and Eu_2CuO_4 in the $z(xx)\bar{z}$ ($A_{1g}+B_{1g}$) pseudobackscattering geometry. Laser energies are indicated in eV.

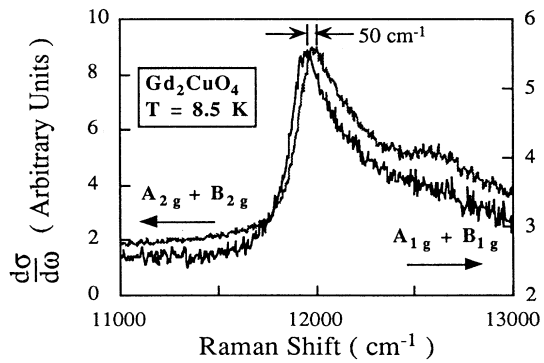

FIG. 11. The A_{1g} and A_{2g} Raman features in Gd_2CuO_4 at 8.5 K with the laser at 363.8 nm (3.41 eV). The two spectra are plotted with different vertical scales as shown to illustrate the 50 cm^{-1} splitting between the two peaks.

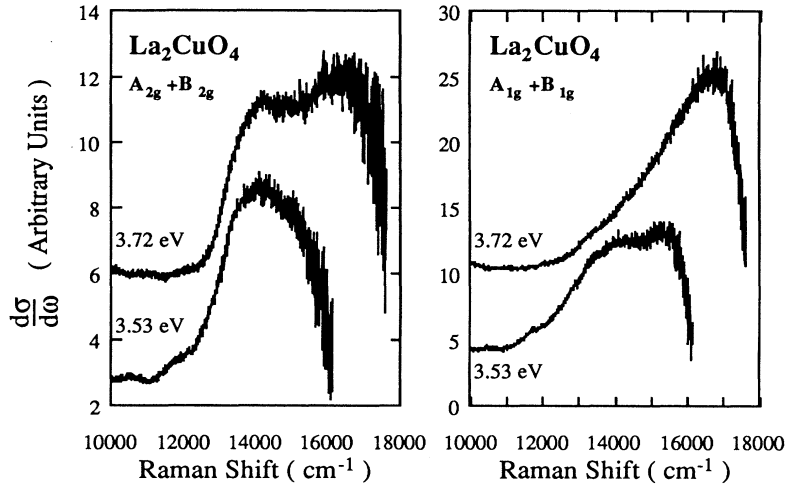

FIG. 12. Room-temperature data on La_2CuO_4 in the $z(xy)\bar{z}$ and $z(xx)\bar{z}$ pseudobackscattering geometries for two different laser lines.

line. In addition, our La_2CuO_4 sample had a surface with many facets, leading to increased stray light and luminescence problems.

Figure 12 shows spectra from La_2CuO_4 at room temperature in the $z(xy)\bar{z}$ and $z(xx)\bar{z}$ pseudo-backscattering geometries. There is an A_{2g} feature near 14 000 cm^{-1} in the $z(xy)\bar{z}$ spectrum, but it is poorly defined because of luminescence. This same luminescence is clearly visible in the $z(xx)\bar{z}$ spectrum where the peak position shifts with wavelength. When plotted versus absolute energy, the two peaks in the $z(xx)\bar{z}$ spectrum line up very well. There seem to be no A_{1g} or B_{1g} Raman features present. With a $z(xx)\bar{z}$ spectrum consisting of almost pure unpolarized luminescence, it is very tempting to simply subtract it from the $z(xy)\bar{z}$ spectrum to leave only the Raman signal. Figure 13 shows the result of doing this for the 3.72-eV line of Fig. 12. The background level no longer has any meaning, but now we can clearly see the pure A_{2g} Raman peak at 13 740 cm^{-1}.

The low-temperature behavior of La_2CuO_4 is also complicated by the presence of luminescence, but knowledge of the room-temperature peak position allows us to make a good interpretation of the data. As shown in Fig. 14, the single room-temperature A_{2g} peak at 13 740 cm^{-1} develops sidebands in a similar fashion to the T' materials. These features are not distinctly resolved in La_2CuO_4, however, and instead the main peak and sidebands are merged together. The dotted lines in the $z(xy)\bar{z}$ spectrum mark the main peak, which is unchanged from its room-temperature position, as well as the first sideband at 14 340 cm^{-1} and the second sideband at 15 360 cm^{-1}. The separations between the main peak and sidebands are remarkably consistent with values from the T' series. Again there seem to be no A_{1g} or B_{1g} features present in the $z(xx)\bar{z}$ spectrum, but there is clear luminescence at around 1.9 eV (14 400 cm^{-1} in the 3.72-eV spectrum, 13 300 cm^{-1} in the 3.3-eV spectrum), close to the energy of the charge-transfer gap.

The resonant behavior of La_2CuO_4 is somewhat complicated by the limits of our detection system. As shown in Fig. 12, there seems to be little or no resonant behavior of the A_{2g} feature at room temperature, but the data with the 3.41-eV laser line are too weak to tell. In Fig. 14, however, there is some evidence for resonant behavior at 5.7 K toward photon energies higher than 3.72 eV. Again, the 3.41-eV spectrum is not entirely trustworthy because of our poor infrared system response. Since there is not much difference in amplitude between the spectra at 3.53 and 3.72 eV, the case for resonant behavior is rather weak. Certainly there is no dramatic enhancement of the A_{2g} features on the scale seen in the T' materials. This seems to indicate that the absolute energy of the charge-transfer gap is very important in the A_{2g} resonance.

C. 123-phase materials

We measured two different insulating 123 samples for this study, $YBa_2Cu_3O_6$ and $PrBa_2Cu_3O_6$. Both of these materials exhibit clear A_{2g} peaks below the optical conductivity maximum as shown in the $z(xy)\bar{z}$ spectrum of Fig. 15. The spacing from the optical conductivity peak is around 1300 cm^{-1} for $YBa_2Cu_3O_6$ and 1600 cm^{-1} for $PrBa_2Cu_3O_6$, somewhat smaller than in the T' series and in La_2CuO_4. Unfortunately, low-temperature optical conductivity data for the 123 materials were not available

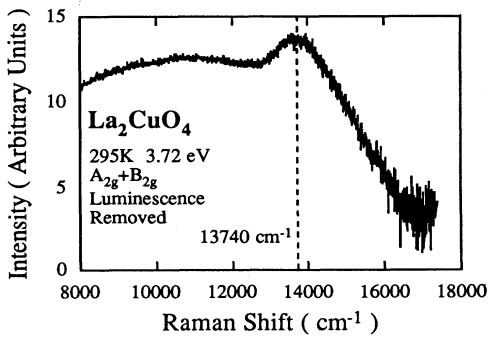

FIG. 13. The spectrum that results from subtracting the 3.72 eV $z(xx)\bar{z}$ data from the $z(xy)\bar{z}$ data in Fig. 12 to remove the luminescence. Now the position of the A_{2g} peak is clear.

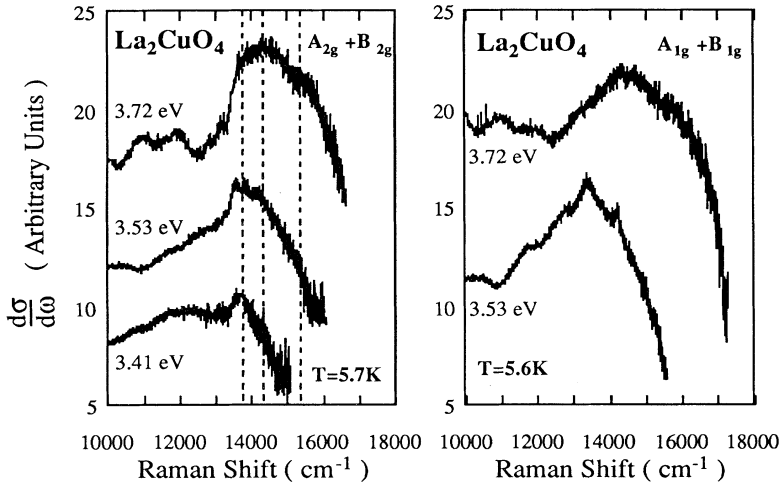

FIG. 14. Low-temperature data at 5.7 K on La_2CuO_4 in the $z(xy)\bar{z}$ and $z(xx)\bar{z}$ pseudobackscattering geometries for three different laser lines. Group representations are indicated assuming tetragonal symmetry. The dotted lines in the $z(xy)\bar{z}$ spectrum show the positions of the main A_{2g} peak and two sidebands.

to make an accurate comparison. Figure 16 shows a Raman symmetry study for $YBa_2Cu_3O_6$, which proves the A_{2g} nature of the main peak and also identifies an additional peak with A_{1g} symmetry at 14 880 cm^{-1}. There are also some possible very weak B_{1g} features near 13 000 and 14 000 cm^{-1}. There seems to be no equivalent for the 14 880-cm^{-1} A_{1g} peak in any of the other insulating cuprates, including $PrBa_2Cu_3O_6$ which has no A_{1g} or B_{1g} features.

Figure 17 shows the $z(xy)\bar{z}$ spectra for $YBa_2Cu_3O_6$ at room temperature and 5.6 K. At first there appears to be a shift in the position of the A_{2g} peak with laser line. In fact what is happening is slightly more subtle. Just as in La_2CuO_4, we are seeing a main peak and two sidebands which are merged together and difficult to resolve. At both temperatures in Fig. 17, however, there is a resonance occurring which is different for each of the sidebands; this changes the overall shape and position of the A_{2g} "peak" between the laser lines. All of the A_{2g} features seem to resonant toward photon energies higher than 3.72 eV, but the resonance seems to be much stronger for the two sidebands than for the main peak, and also stronger at 5.6 K than at room temperature.

As a result of this resonance and the limits of our detection system, the 3.41-eV spectrum at both temperatures in Fig. 17 shows almost exclusively the main A_{2g} peak, centered at 12 460 cm^{-1}. The two sidebands can then be identified as they grow in intensity in the 3.53 and 3.72 eV spectra, as illustrated by the dotted lines in Fig. 17. The sideband positions at 13 060 and 14 090 cm^{-1} give spacings of 600 and 1630 cm^{-1} from the main peak, spacings remarkably similar to all of the other insulating cuprates. There also seems to be another sideband present at 14 730 cm^{-1} in the low-temperature 3.72-eV spectrum of Fig. 17. Such a third sideband has not been resolved in the other insulating cuprates, but it occurs at a spacing of 2280 cm^{-1} from the main A_{2g} peak, which is remarkably close to the sum of the spacings of the first two sidebands ($600+1630=2230$ cm^{-1}). We can thus assign the third sideband as combination scattering from the first two excitations.

Figure 18 shows resonance data from $YBa_2Cu_3O_6$ in the $z(xx)\bar{z}$ pseudo-backscattering geometry. It is clear that the A_{1g} peak at 14 880 cm^{-1} resonates very strongly at 5.7 K near the 3.72-eV laser line. Additionally, there seems to be a weak Raman feature at 14 240 cm^{-1} as indicated by the dotted line in the 5.7-K spectrum and the arrow in the 295-K spectrum. There is no conclusive evidence here for any of the possible B_{1g} features mentioned earlier. At 295 K, the very intense rising spectrum that shifts with the laser line seems to be luminescence below the charge-transfer gap. The gap appears at about 14 700 cm^{-1} in the 3.53-eV spectrum and 13 700 cm^{-1} in the 3.41-eV spectrum. In each case, both values seem to be above the highest luminescence edge. Such behavior is consistent with the luminescence around 1.3 eV observed in $YBa_2Cu_3O_6$.[42] Our detector sensitivity does not, however, permit us to look far enough into the infrared to find the actual peak in the luminescence.

Unfortunately, luminescence turns out to be a significant problem in $PrBa_2Cu_3O_6$, as shown in Fig. 19.

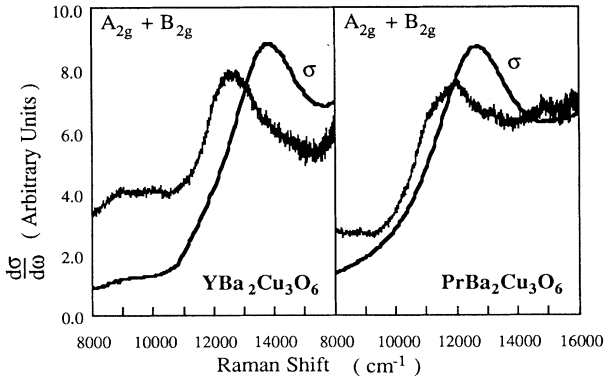

FIG. 15. Raman scattering in the $z(xy)\bar{z}$ pseudobackscattering geometry at room temperature with the laser at 333.6 nm (3.72 eV). Spectra are shown for an etched sample of $YBa_2Cu_3O_6$ as well as $PrBa_2Cu_3O_6$. Also plotted with a different vertical scale is the optical conductivity.

Just as in La_2CuO_4 and $YBa_2Cu_3O_6$ there seem to be multiple A_{2g} peaks merged together, but the presence of strong luminescence obscures their position. Since the $z(xx)\bar{z}$ spectrum appears to mostly luminescence common to the $z(xy)\bar{z}$ (see Fig. 21), we can make use of the same technique as in La_2CuO_4 and subtract away the luminescence to find the peak positions. Figure 20 shows the resulting spectrum, in which the main A_{2g} peak at 11 060 cm^{-1} and the first sideband at 11 710 cm^{-1} become well resolved. These positions have been indicated in Fig. 19 with dotted lines, along with the probable location of the second sideband, at 12 680 cm^{-1}. The positions and spacings of all of these A_{2g} features are consistent with the other insulating cuprates.

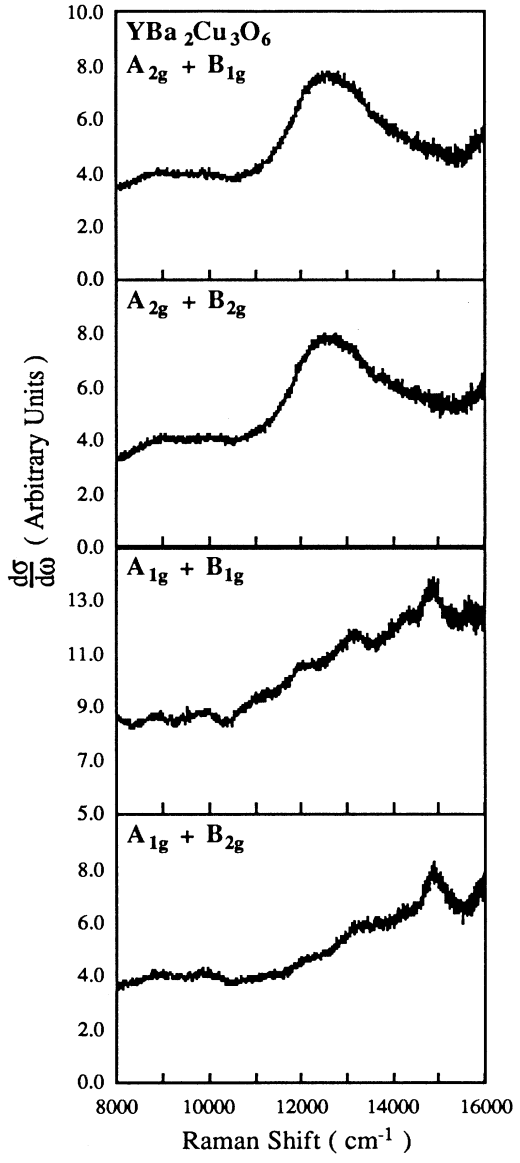

FIG. 16. Symmetry study of Raman features at room temperature in $YBa_2Cu_3O_6$. The laser was at 333.6 nm (3.72 eV) in the pseudobackscattering configuration. Spectra are shown for the $z(x'y')\bar{z}$ ($A_{2g}+B_{1g}$), $z(xy)\bar{z}$ ($A_{2g}+B_{2g}$), $z(xx)\bar{z}$ ($A_{1g}+B_{1g}$), and $z(x'x')\bar{z}$ ($A_{1g}+B_{2g}$) scattering geometries.

Figure 21 shows the $z(xx)\bar{z}$ pseudobackscattering geometry on $PrBa_2Cu_3O_6$ at both 7 K and room temperature. The way all the observed features clearly shift in position with laser energy is a good indication they result from luminescence. The luminescence peak in the 295 K spectrum is close to 14 340 cm^{-1} (1.78 eV), considerably above the optical conductivity peak at 12 640 cm^{-1} (1.57 eV). It is tempting to call the sharper peak near 15 000 cm^{-1} in the 7.4 K 3.72-eV spectrum a Raman A_{1g} feature by analogy with $YBa_2Cu_3O_6$. Plotting the 7.4 K data versus an absolute wave-number scale in Fig. 22 however, illustrates that this feature is more likely a luminescence peak near 15 110 cm^{-1} (1.87 eV), as shown by the dotted line. The actual peak position may be lower in energy since our detector sensitivity runs out on the falling edge of the luminescence. Two additional luminescence peaks are also resolvable in Fig. 22 at 15 740 and 16 580 cm^{-1} (1.95 and 2.06 eV), again marked by dotted lines. The origin of these states above the optical conductivity peak is unclear.

IV. DISCUSSION OF RESULTS

A. Summary of experimental results

The results of the previous section bring to light a number of important trends. As shown in Fig. 23, we have observed three A_{2g} features in all of the insulating cuprates studied: a main peak and two sidebands. The spacings between the main peak and the first sideband, around 600 cm^{-1}, and between the main peak and the second sideband, around 1500 cm^{-1}, seem to remain relatively constant throughout the insulating cuprates. Since the T and 123-phase materials have "apical" oxygens while T'-phase materials do not, Fig. 23 shows that the apical oxygens do not play a role in the A_{2g} mechanism. More importantly, it shows that the A_{2g} mechanism is independent of the oxygen coordination number on the in-plane copper atoms.

Figure 23 also shows curves plotted for each of the peaks based on a least-squares fit to the data. The functional form of the fit was the power-law relation $\omega=\omega_0(d/d_0)^{-n}$, which gives better fits than a linear relation. Such a power-law relation is also expected between the copper-oxygen charge-transfer energy and the in-plane bond length d. The fit parameters are shown in Table I, where the parameter d_0 is the shortest bond length in the sample series, that of La_2CuO_4 at 1.907 Å.[15] The exponents found for all three A_{2g} features deviate by at most 6% from each other, well within experimental error. The exponent found for the optical conductivity peak is significantly different, however, leading to the conclusion that the processes involved are probably different than for the A_{2g} peaks.

It is also interesting to compare the fitted exponents for the A_{2g} peaks with those measured for the two-magnon and two-phonon Raman peaks. Since it is known[43] that there is a linear relationship between hydrostatic pressure and copper-oxygen bond length in La_2CuO_4, we can compare our data with pressure dependence study of Aronson

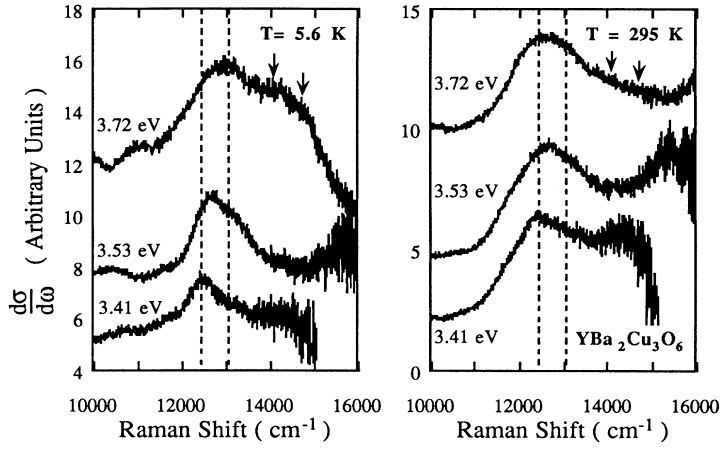

FIG. 17. Raman scattering from an etched sample of $YBa_2Cu_3O_6$ in the $z(xy)\bar{z}$ $(A_{2g}+B_{2g})$ pseudobackscattering geometry at two temperatures. Spectra are shown for three different laser energies. Dotted lines indicate the positions of the main A_{2g} peak and first sideband; arrows indicate the positions of the second and possible third sidebands.

et al.[44] They find a similar power-law relationship between the exchange parameter J and the copper-oxygen bond length d with an exponent of n of 6.4 ± 0.8 over a 2.5% variation in d. This agrees reasonably well with our A_{2g} results over a variation in d of about 3.5%, possibly indicating that the two-magnon and A_{2g} intermediate states are related.

Pressure dependence studies of Eremets *et al.*[45] and Maksimov and Tartakovskii[46] report an exponent of 3 ± 0.5 for Eu_2CuO_4 and $YBa_2Cu_3O_{6.2}$, but this is over a wider pressure range (variation in d of 10%), and there is evidence that the power-law changes to a lower exponent at pressures higher than 80 kbar (variations in d of greater than $\sim2.3\%$).[44] Uzumaki *et al.*[15] report two-magnon and two-phonon exponents of 4.6 and 6.3, respectively, for all the T and T' materials, but their two-magnon curve fits very poorly with their value for La_2CuO_4. Their two-phonon fitted curve aligns with their La_2CuO_4 value, however, and the fitted two-phonon exponent at 6.3 agrees well with Table I. Thus the fitted exponents for our data seem consistent with both the two-magnon and two-phonon features.

We can also use the fitting results of Table I to estimate the expected temperature shift of the main A_{2g} peak between room and liquid-helium temperatures. Using the low-temperature lattice constants for Nd_2CuO_4,[47] Pr_2CuO_4,[48] and La_2CuO_4,[27,49] we find that the 295-K peaks should shift 66, 64, and 96 cm^{-1}, respectively, toward higher energies at ~10 K. Because the room-temperature A_{2g} peaks are so broad, however, this displacement is well within our experimental error. Thus we cannot draw any firm conclusions about the temperature dependence of the A_{2g} peak positions.

For the case of the broad B_{1g} symmetry feature observed in all of the T'-phase materials, there seems to be a consistent shift of around 500 cm^{-1} to higher energies between 295 and 150 K, with no further shifts below 150 K. This behavior exactly mimics that of the optical conductivity peak with temperature, indicating that the B_{1g} feature and the band-edge optical states are closely related. The different displacements with temperature would also seem to indicate that the A_{2g} peaks and the B_{1g} feature arise through different scattering mechanisms. The absence of a B_{1g} feature in the T- and 123-phase materials may mean the apical oxygens play a role in suppressing or destroying the B_{1g}-symmetry scattering process.

The full resonance behavior of the large-shift Raman features is difficult to ascertain without additional laser lines. Some trends seem clear, however. The A_{2g} peaks in all of the insulating cuprates show almost no resonance at room temperature, or only a slight resonance toward photon energies beyond 3.72 eV. At low temperatures, there seems to be a fairly consistent resonance toward energies below 3.41 eV in the T' series and energies above 3.72 eV in the T and 123 phases. Such behavior points to involvement of the apical oxygens in shifting the energies of the A_{2g} scattering process intermediate states. The B_{1g} feature in the T' series shows consistent weak resonance toward energies above 3.72 eV, even at low temperatures. This is further evidence that the scattering mechanisms are different for the A_{2g} and B_{1g} features.

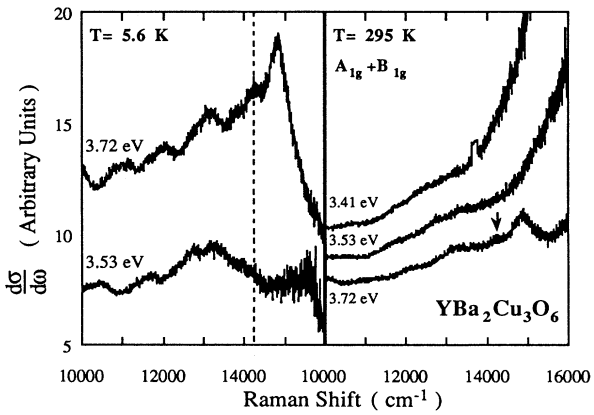

FIG. 18. Raman scattering from an etched sample of $YBa_2Cu_3O_6$ in the $z(xx)\bar{z}$ $(A_{1g}+B_{1g})$ pseudobackscattering geometry at two temperatures. Spectra are shown for three different laser energies. The dotted line in the 5.6 K spectrum shows the location of a second weak Raman peak at 14 730 cm^{-1}; the arrow in the 295 K spectrum points to the same position.

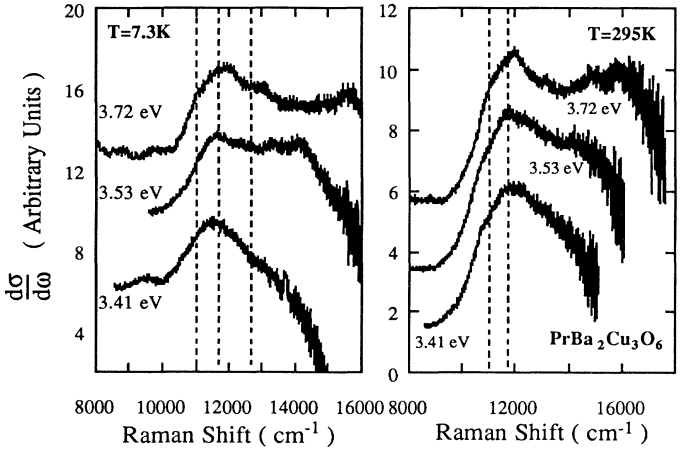

FIG. 19. Raman scattering from $PrBa_2Cu_3O_6$ in the $z(xy)\bar{z}$ ($A_{2g}+B_{2g}$) pseudobackscattering geometry at two temperatures. Spectra are shown for three different laser energies. Dotted lines indicate the positions of the main A_{2g} peak and two sidebands.

There are additionally two different A_{1g} peaks observed, one that appears just below the A_{2g} peak position in only Gd_2CuO_4 (50 cm^{-1} below) and Eu_2CuO_4 (40 cm^{-1} below), and one that appears in $YBa_2Cu_3O_6$ and possibly in $PrBa_2Cu_3O_6$ near 14 880 cm^{-1} (around 2200 cm^{-1} above the A_{2g} main peak). While the origin of the $YBa_2Cu_3O_6$ peak is not clear, the Gd_2CuO_4 and Eu_2CuO_4 peaks seem to be correlated with the previously mentioned in-plane oxygen distortion present in these materials and not in any of the others studied here. The amplitude of the A_{1g} peak is stronger in Gd_2CuO_4 than in Eu_2CuO_4, corresponding to the stronger distortion present in Gd_2CuO_4.[36,37,41]

There are also several indications that the A_{1g} peaks in Gd_2CuO_4 and Eu_2CuO_4 are directly related to the A_{2g} peaks. First, the A_{1g} peaks maintain a constant fixed distance from the main A_{2g} peak and do not shift with temperature, although this is hard to tell at temperatures higher than about 70 K since both peaks broaden considerably. Second, although the intensity of the A_{1g} peaks seems to increase dramatically at low temperatures, its resonance characteristics are the same as those of the main A_{2g} peak. Finally, when the A_{1g} and A_{2g} peaks are plotted together and overlapped for Gd_2CuO_4, their line shapes are almost identical, as shown in Fig. 11. A similar situation seems to exist for Eu_2CuO_4, although the A_{1g} peak is too weak to tell with certainty. Thus, the A_{1g} and A_{2g} peaks both seem to arise from the same scattering process in Gd_2CuO_4 and Eu_2CuO_4, with some kind of distortion-induced splitting that changes the symmetry.

B. The *d-d* transition model

There are certainly many interpretations of the above results. One recent proposal[50] involves "hole-doublons," or electron-hole pairs in a bound state moving on only one of the two sublattices and accompanied by a spin excitation in the form of a "hedgehog." Here, however, we will concentrate on another model which seems to explain our A_{2g} peaks particularly well. Note that this model does not account for the B_{1g} peak observed in the T' materials, as that feature seems to involve a different coupling mechanism from the A_{2g} peaks. Nor does this model account for the A_{1g} peak observed in $YBa_2Cu_3O_6$, since limitations on our detector sensitivity in the infrared have prevented detailed study of that feature. Bearing these facts in mind, we will concentrate on the A_{2g} and T' A_{1g} peaks, which all seem to arise from the same phenomena.

The basic premise for our *d-d* transition model is that the main A_{2g} peak arises from electronic scattering between two in-plane copper $3d$ levels. In particular, a transition between the occupied $d_{x^2-y^2}$ level and the unoccupied d_{xy} level (in the hole picture) would transform as the function $xy(x^2-y^2)$, which has A_{2g} symmetry. It is important to note that the d_{xy} orbital symmetry is also the same as a ring of oxygen p_π orbitals phased as in Fig. 24. As a result, the copper d_{xy} orbital is likely to hybridize with the oxygen p_π orbitals, and it is this admixed hybrid orbital with largely d_{xy} character that is the final state of the hole.

Three pieces of evidence support our *d-d* transition model. First, although the energy splitting between the

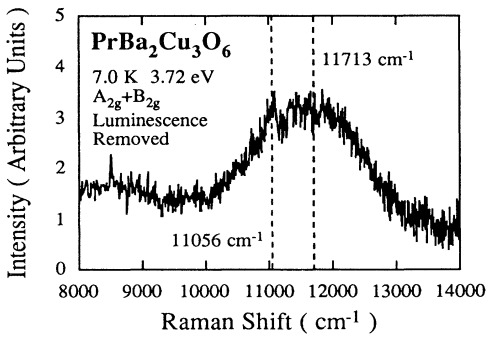

FIG. 20. The spectrum that results from subtracting the 7.4 K 3.72-eV $z(xx)\bar{z}$ data in Fig. 21 from the corresponding $z(xy)\bar{z}$ data in Fig. 19 to remove the luminescence. Now the positions of the A_{2g} peak and first sideband are more clearly resolved.

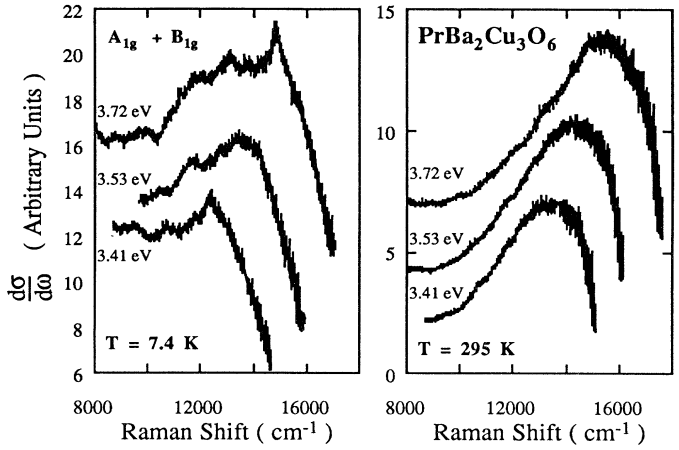

FIG. 21. Raman scattering from $PrBa_2Cu_3O_6$ in the $z(xx)\bar{z}$ ($A_{1g}+B_{1g}$) pseudobackscattering geometry at two temperatures. Spectra are shown for three different laser energies.

$d_{x^2-y^2}$ and d_{xy} levels has not been positively determined, cluster[51,52] and local-density functional[53] calculations for La_2CuO_4 predict a splitting of around 1.4–1.9 eV, very close to our main A_{2g} peak energy of 1.70 eV (13 740 cm^{-1}). Several recent experiments also suggest that the *d-d* transition should lie in this energy range. For example, midinfrared electroreflectance measurements[54] on La_2CuO_4 find a peak near 1.5 eV which has the correct symmetry for this transition. Absorption measurements[55] on the similar material $Sr_2CuO_2Cl_2$ find an absorption edge around 1.5 eV which the authors suggest corresponds to $d_{x^2-y^2}$ and d_{xy} transitions. Additionally, photoconductivity measurements[56] on $YBa_2Cu_3O_{6.0}$ thin films show a shoulder near 1.5 eV, below the main conductivity peak. All of the above energies are in good agreement with our main A_{2g} peak positions of 1.4–1.7 eV.

Second, an intra-*d*-level transition would be expected to scale with copper-oxygen bond distance, as we observed for the A_{2g} peak, because this affects the orbital hybridization and crystal-field splitting energies. To first order, the d_{xy} to $d_{x^2-y^2}$ splitting is proportional to the A_{2g} term $\sin(4\phi)[r^4/d^5]$, where ϕ is the azimuthal angle, leading to a negative power-law exponent of 5 for variations in copper-oxygen bond distance d. This is in fair agreement with our values of Table I, and the difference may be a result of hybridization effects. Finally, a *d*-level transition would be relatively insensitive to changes in temperature or the presence of apical oxygens. This is also in agreement with our A_{2g} peak, where we find little or no energy shift with temperature and only bond-length-related energy shifts among the T', T, and 123 structure materials.

In our picture of the $d_{x^2-y^2}$ to d_{xy} transition there are several possible intermediate states. Here we discuss only photon-induced charge transfer among *d* orbitals. Later

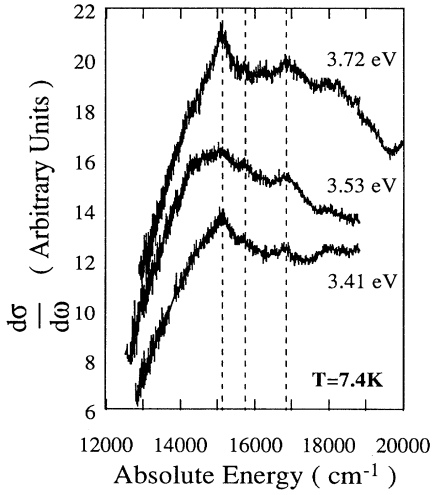

FIG. 22. The same 7.4 K data from Fig. 21 is replotted here vs an energy scale of absolute wave numbers. Features that line up in this plot are luminescence. Three peaks are indicated with dotted lines.

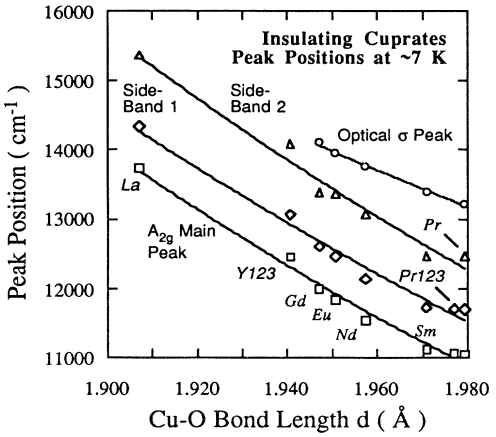

FIG. 23. The positions of the main A_{2g} peak and two sidebands at ~7 K, plotted versus the 295 K value of the in-plane copper-oxygen bond length for all the insulating cuprates. For the T' series, the peak positions for the optical conductivity at 10 K are also shown. All data have been fit to a power-law relation of the form $\omega=\omega_0(d/d_0)^{-n}$, where the fitting parameters are shown in Table I.

TABLE I. Least-squares-fit parameters from Fig. 23 for the power-law relation $\omega=\omega_0(d/d_0)^{-n}$. The regression coefficient R measures the goodness of fit, with 1.0 being a perfect fit. The parameter d_0 was chosen as the copper-oxygen bond length of La_2CuO_4 at 1.907 Å, the shortest in this study.

Raman feature	ω_0	n	R
A_{2g} main peak	13 690	6.075	0.992 8
Sideband 1	14 280	5.683	0.990 8
Sideband 2	15 350	5.967	0.987 0
Optical σ peak	15 250	3.887	0.997 4

we will introduce d-p charge transfer. Let us assume that the intermediate state is reached, as shown in Fig. 25(b), by photon assisted charge transfer of a down-spin hole from an occupied $d_{x^2-y^2}$ orbital at the central site to the same orbital on the copper site immediately to the left, induced by x-polarized light. The material is (at least locally) antiferromagnetically ordered, and the two holes in the $d_{x^2-y^2}$ orbital on the left-hand side have opposite spins. There are two possible final states that can be induced by y-polarized light acting on the doubly occupied $d_{x^2-y^2}$ state on the left-hand copper site, shown in Figs. 25(c) and 25(d). In the first, a down-spin hole is transferred to the d_{xy} orbital on the central site. The net effect is then transfer of a down spin from the $d_{x^2-y^2}$ orbital to the d_{xy} orbital on the central site. This process would account for the main A_{2g} peak. The second possibility is for the up-spin hole to be transferred to the d_{xy} orbital on the central site. This process would involve double spin flip (or two-magnon creation) in addition to the A_{2g} excitation.

In a simple Ising-type calculation, the energy of the second final state would be raised above the first according to the number of bonds changed from antiferromagnetic to ferromagnetic as a result of the spin-exchange process. By examining Fig. 25(d), it is evident that the flipped spin on the left-hand site sees three wrong bonds, each costing an energy of $\frac{1}{2}J$. The flipped spin of the d_{xy} hole on the central site also sees three wrong bonds, but the cost is essentially zero, because symmetry considerations rule out (super)exchange between d_{xy} and $d_{x^2-y^2}$ orbitals on first-neighbor sites of the square lattice. Thus the second final state would rise in energy above the first final state by around $\frac{3}{2}J$, or about 1500 cm^{-1}, which is similar to our observed second sideband offset. Since the charge-transfer process leading to this new type of two-magnon excitation can occur between any pair of nearest-neighbor copper sites, it has an effective symmetry of A_{1g}. The d-d transition that is the activation process must have A_{2g} symmetry, however, so the effective symmetry of the coupled process must be $A_{1g}\otimes A_{2g}=A_{2g}$.

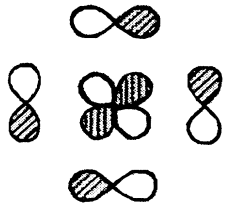

FIG. 24. The phasing of the oxygen p_π orbitals shown here gives a large overlap with the copper d_{xy} states. As a result, there will likely be some amount of hybridization between the oxygen p_π and copper d_{xy} orbitals.

Ordinarily, two-magnon scattering with A_{1g} symmetry is forbidden in the Heisenberg spin-$\frac{1}{2}$ system, because the light-scattering Hamiltonian is proportional to the Hamiltonian for the system, precluding off-diagonal states.[57] In the present case, the two-magnon excitation is accompanied by an on-site d-d transition, which is not accounted for in the Heisenberg Hamiltonian. It therefore seems likely that the second sideband is two-magnon scattering under this new process.

The energy of the first sideband at $\sim$600 cm^{-1} bears a remarkable similarity to that of the Raman-activated E_u phonon seen in all the insulating cuprates.[30–32,36,37] This phonon is known to be an in-plane TO copper-oxygen stretching mode,[58] which means it could easily couple to charge-transfer processes. The observed symmetry of this normally Raman-forbidden phonon appears mixed in some of the insulators,[31] but it is consistently more intense in the A_{1g} geometry. (It only appears in this geometry for $YBa_2Cu_3O_6$, for example.[32]) Assuming that the phonon has A_{1g} symmetry, the coupled phonon and d-d transition process would then appear with $A_{1g}\otimes A_{2g}=A_{2g}$ symmetry, so that both the energy and symmetry are in good agreement with our first A_{2g} sideband. Additionally, the power-law dependence of the two-phonon feature with copper-oxygen bond length reported by Uzumaki *et al.*[15] matches fairly well with the first sideband value listed in Table I.

The A_{1g} feature in Gd_2CuO_4 and Eu_2CuO_4 can also be explained within the d-d transition model. As mentioned previously, both of these materials are known to have slight in-plane oxygen distortions with B_{1g} symmetry about the center of the unit cell.[35] These distortions produce B_{1g} symmetry phonon peaks in Raman scattering.[36,37] If we look at the symmetry of the oxygen distortion around a copper site, however, it becomes clear that there is an effective rotation of the oxygen atoms alternating between clockwise and counterclockwise directions along a line of copper sites; such a rotation has A_{2g} symmetry about each copper atom.

C. The role of oxygen p_σ and p_π orbitals

In the distorted state there are two copper sites per unit cell. These are nearest neighbors on the Cu lattice; they have opposite spin in the Néel ground state and have opposite senses of the rotation of their four oxygen neighbors in the distorted state. The A_{2g} excitation for zero wave vector corresponds to an in-phase superposition of $d_{x^2-y^2}$ to d_{xy} hole excitations on the two Cu sites in the unit cell. The A_{1g} excitation corresponds to the out-of-phase $d_{x^2-y^2}$ to d_{xy} hole excitation. The difference in en-

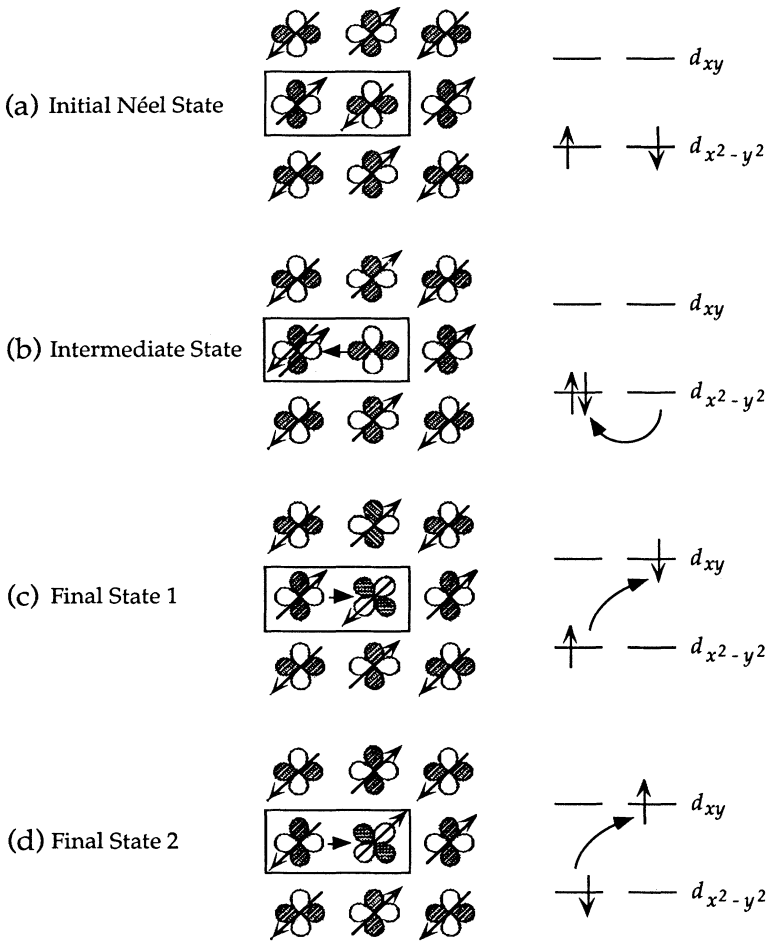

FIG. 25. Illustration of the *d-d* mechanism for A_{2g} Raman scattering in the hole picture. The lattice here is assumed to be initially in the Néel state, as illustrated in (a) with holes represented as arrows. Excitation by *x*-polarized light induces a charge transfer of a down-spin hole from the central copper site $d_{x^2-y^2}$ orbital to the $d_{x^2-y^2}$ orbital on the site immediately at left, leading to the intermediate state shown in (b). Excitation by *y*-polarized light can then induce two possible final states. In (c) a down-spin hole is transferred from the $d_{x^2-y^2}$ orbital on the site at left to the d_{xy} orbital on the central site. This restores the Néel ordering, and the total cost is thus only the *d-d* level energy difference. In (d), an up-spin hole is transferred from the $d_{x^2-y^2}$ orbital on the site at left to the d_{xy} orbital on the central site. This involves an effective double spin-flip, and the total cost is thus the *d-d* level energy difference as well as the energy of three exchange interactions.

ergy between these excitations is due to the exchange energy between $d_{x^2-y^2}$ and d_{xy} orbitals on the two different copper sites in the unit cell. Direct exchange is negligibly small. Superexchange results from hybridization of $d_{x^2-y^2}$ and d_{xy} with p_σ and p_π oxygen orbitals, respectively. The exchange interaction between the hybridized oribtals then occurs through the exchange integral between p_σ and p_π orbitals on the oxygen site that is the common first neighbor to the two copper sites in the unit cell. We first discuss the nature of these states in the undistorted lattice. Next we discuss a *d-p* model for Raman scattering which predicts two resonances and which shows how the distortion induces Raman activity in the A_{1g} excitation.

Let $j=1,2$ label the two sites in the unit cell where the spin is normally up and down, respectively. Site 1 has four nearest neighbors on the same magnetic lattice as site 2, all of which are excited in phase. We will calculate the energy splitting between symmetric and antisymmetric *d-d* excitations on sites 1 and 2. The total energy splitting in the lattice will be four times this value. From the four oxygen p_σ orbitals that are nearest neighbors to each Cu site form the normalized linear combination that has the same nodal structures as $d_{x^2-y^2}$. Denote this by P_σ. From the four oxygen p_π orbitals that are nearest neighbors to each Cu site form the normalized linear combination that has the same nodal structure as d_{xy}, as shown in Fig. 24. Denote this by P_π. Denote the $d_{x^2-y^2}$ and d_{xy} orbitals by e and t, respectively. Then the hybridized states that replace e and t take the form

$$E(j)=e(j)\cos\theta+P_\sigma(j)\sin\theta=\frac{(-1)^j}{2}p_\sigma(0)\sin\theta+\cdots\ , \tag{1a}$$

$$T(j)=t(j)\cos\phi+P_\pi(j)\sin\phi=\frac{(-1)^j}{2}p_\pi(0)\sin\phi+\cdots\ , \tag{1b}$$

where θ and ϕ are mixing angles. The second equalities show how these states depend on the p orbitals on the oxygen site (0) lying between Cu(1) and Cu(2).

We must consider the two-hole final states $E_\uparrow(1)T_\downarrow(2)$, where the down-spin hole in site 2 is excited from E to T, and $T_\uparrow(1)E_\downarrow(2)$, where the up-spin hole on site 1 is excited. These degenerate states are coupled by superexchange. The final states of the "*d-d*" transition are then

$$|\pm\rangle \equiv \frac{1}{\sqrt{2}}[E_\uparrow(1)T_\downarrow(2) \pm T_\uparrow(1)E_\downarrow(2)]$$
$$= -\frac{1}{4\sqrt{2}}\sin\theta\sin\phi[p_{\uparrow\sigma}(0)p_{\downarrow\pi}(0) \pm p_{\uparrow\pi}(0)p_{\downarrow\sigma}(0)] + \cdots , \quad (2)$$

where the subscripts $\uparrow, \downarrow$ denote spin. The second equality shows only that portion dependent on $p(0)$ orbitals. These states $|\pm\rangle$ have a contribution of p orbitals to the Coulomb energy given by

$$\langle +|H_c'|+\rangle = \tfrac{1}{16}\sin^2\phi\sin^2\theta[U(p_\sigma,p_\pi)+K(p_\sigma,p_\pi)] , \quad (3a)$$

$$\langle -|H_c'|-\rangle = \tfrac{1}{16}\sin^2\phi\sin^2\theta[U(p_\sigma,p_\pi)-K(p_\sigma,p_\pi)] , \quad (3b)$$

where $U(p_\sigma,p_\pi)$ is the Coulomb repulsive energy if there is one hole on a p_σ orbital and one on a p_π orbital on the same oxygen site and where $K(p_\sigma,p_\pi)$ is the exchange integral between these two orbitals. Taking the difference and multiplying by four, we see that the odd-phased state is lower in energy than the even-phased state by the amount

$$\delta E = \tfrac{1}{2}\sin^2\phi\sin^2\theta K(p_\sigma,p_\pi) . \quad (4)$$

Using the value of $K(p_\sigma,p_\pi)=0.83$ eV from Grant and McMahan,[59] we obtain agreement with the observed splitting of about 6 meV if the mixing angles obey $|\sin\phi\sin\theta| \approx \frac{1}{8}$.

Thus, the "minimalist model" necessary to explain the A_{1g} peak in the d-d picture requires four sets of orbitals: $d_{x^2-y^2}$ (e), d_{xy} (t), p_σ, and p_π. Note that we neglect other orbitals such as $d_{3z^2-r^2}$ which are usually included in multiband calculations of electronic structure in cuprates; indeed the latter are usually assigned more importance than d_{xy}.

We now present a "minimalist" discussion of the resonance-Raman effect, neglecting hybridization between e, t, p_σ, and p_π. Define the hole energy differences

$$\Delta = E(p_\sigma) - E(e) , \quad (5)$$

$$\delta = E(p_\pi) - E(p_\sigma) , \quad (6)$$

both of which are assumed to be positive. Denote by $\mathbf{x}$ and $\mathbf{y}$ the unit vectors along x and y axes, and denote the rotation angle of the Cu-O bonds due to the distortion by ϵ. In this calculation we let the operator j_x produce the intermediate state and the operator j_y produce the final state for A_{2g} (j_x for A_{1g}). The initial hole state is $e(0)$, i.e., $d_{x^2-y^2}$ at the origin; the intermediate states are, to first order in ϵ, p_x at $\pm a_0(\mathbf{x}+\epsilon\mathbf{y})$, i.e., p_σ, and p_x at $\pm a_0(\mathbf{y}-\epsilon\mathbf{x})$, i.e., p_π; and the final state is $t(0)$. Here a_0 is the Cu-O bond length. The results of second-order perturbation theory for the Raman matrix elements are, to first order in ϵ:

$$A_{2g}(yx): \quad \frac{-2ac}{\Delta - E_L} - \frac{2df}{\Delta+\delta-E_L} , \quad (7)$$

$$A_{1g}(xx): \quad \frac{2ab\epsilon}{\Delta - E_L} + \frac{2dg\epsilon}{\Delta+\delta-E_L} , \quad (8)$$

where E_L is the laser photon energy. The matrix elements a-d,f,g are all positive and are given by

$$a = i\langle p_x(a_0\mathbf{x})|j_x|e(0)\rangle , \quad (9a)$$

$$\epsilon b = -i\langle t(0)|j_x|p_x[a_0(\mathbf{x}+\epsilon\mathbf{y})]\rangle , \quad (9b)$$

$$c = i\langle t(0)|j_y|p_x(a_0\mathbf{x})\rangle , \quad (9c)$$

$$d = i\langle p_x(a_0\mathbf{y})|j_x|e(0)\rangle , \quad (9d)$$

$$\epsilon f = -i\langle t(0)|j_x|p_x[a_0(\mathbf{y}-\epsilon\mathbf{x})]\rangle , \quad (9e)$$

$$g = i\langle t(0)|j_y|p_x(a_0\mathbf{y})\rangle , \quad (9f)$$

where $i=\sqrt{-1}$.

The A_{1g} Raman amplitude is proportional to ϵ, which is equal and opposite for the two Cu sites in the unit cell. Equation (8) thus produces a coupling to the d-d "difference mode," the state $|-\rangle$ of Eq. (2).

The resonances at $E_L=\Delta$ in Eqs. (7) and (8) should occur in the 1.6–2.6 eV range where phonon or two-magnon resonant Raman scattering is observed.[19] This agrees reasonably well with our low-temperature T' series data, which show a resonance someplace close to (but at a lower energy than) the 3.41-eV laser line. The resonance at $E_L=\Delta+\delta$ may occur above the range of our experiments, i.e., above 3.8 eV, as suggested by the room-temperature curves in Fig. 8. A more realistic calculation would account for hybridization and band-structure effects; thus, the values of Δ and δ should be regarded as "effective" values.

Within this picture, we would expect the A_{1g} peak to get stronger at lower temperatures, where the oxygen atoms are more localized in the distorted positions. This is in good agreement with our data. We would also expect the intensity ratio of the A_{1g} and A_{2g} peaks to be close to the square of the rotation angle ϵ of the d_{xy} Cu-O bonds. Since the oxygen atoms are known[35] to be displaced by 0.18 Å in Gd_2CuO_4, and the copper oxygen bond distance is 1.947 Å,[15], this angle would be $0.18/1.947 \approx 0.1$ rad. This gives a ratio of roughly 100:1 between the A_{2g} and A_{1g} peak intensities, while the observed ratio in Fig. 11 is close to 2:1. It would be interesting to perform a more detailed calculation.

V. CONCLUSION

We have presented results demonstrating the existence of A_{2g} (pseudovector) symmetry Raman scattering features in all of the T-phase, T'-phase, and 123-phase insulating cuprates. The single A_{2g} peak present at room temperature splits into three or more peaks below 150 K, with spacings of around 600 and 1500 cm^{-1}, respectively, between the lowest-energy (most intense) peak and the two nearest higher-energy sidebands. The energies of

these features consistently below the corresponding peak in optical conductivity, putting them within the charge-transfer gap. Additional peaks with A_{1g} symmetry appear within the gap in Gd_2CuO_4 and Eu_2CuO_4, and above the gap in $YBa_2Cu_3O_6$. A further B_{1g} symmetry feature appears in the T' materials at an energy coinciding with the optical conductivity peak, or gap edge. All of these features resonate toward photon energies above 3.7 eV, except at low temperatures where the T' materials show resonance behavior toward energies below 3.4 eV.

We have presented a model involving copper atom d-d transitions which can explain many of the large-shift Raman features we seen. This model is based on the insight that transitions between copper $d_{x^2-y^2}$ and d_{xy} orbitals are expected to have both the correct A_{2g} symmetry and correct energy difference to account for the main large-shift Raman peaks we have seen. The slightly lower energy A_{1g}-symmetry peak in Gd_2CuO_4 and Eu_2CuO_4, which are distorted by alternating in-plane rotations of CuO_4 units, is attributed to the out-of-phase excitation of d-d transitions on the two copper sites in the magnetic unit cell. The energy lowering is due to superexchange involving p_σ and p_π orbitals. Raman activity is induced by rotation of the Cu-O bonds. We also sketched a picture of resonant Raman scattering for the A_{2g} and sharp A_{1g} peaks in terms of excitations to renormalized p_σ and p_π levels. Should these arguments prove valid, they would have important implications for theoretical models of the insulating state.

ACKNOWLEDGMENTS

We thank the NSF for support under DMR 93-20892 and DMR 90-17156 (D.S., R.L., M.V.K.) and through the Science and Technology Center for Superconductivity under DMR 91-20000 (R.L., S.L.C., M.V.K., W.C.L., D.M.G.).

*Present address: Superconductivity Research Laboratory, ISTEC, Shinonome 1-10-13, Koto-ku, Tokyo 135, Japan.

†Present address: Department of Physics, University of Maryland, College Park, MD 20742.

‡Present address: Department of Physics, Sookmyung University, Seoul, Korea.

[1]J. Zaanen, G. A. Sawatzky, and J. W. Allen, Phys. Rev. Lett. **55**, 418 (1985).

[2]S. L. Herr, K. Kamarás, D. B. Tanner, S.-W. Cheong, G. R. Stewart, and Z. Fisk, Phys. Rev. B **43**, 7847 (1991).

[3]S. L. Cooper, G. A. Thomas, A. J. Millis, P. E. Sulewski, J. Orenstein, D. H. Rapkine, S.-W. Cheong, and P. L. Trevor, Phys. Rev. B **42**, 10 785 (1990).

[4]S. L. Cooper, D. Reznik, A. Kotz, M. A. Karlow, R. Liu, M. V. Klein, W. C. Lee, J. Giapintzakis, and D. M. Ginsberg, Phys. Rev. B **47**, 8233 (1993).

[5]J. Fink, N. Nücker, H. A. Romberg, and J. C. Fuggle, IBM J. Res. Develop. **33**, 372 (1989).

[6]M. Alexander, H. Romberg, N. Nücker, P. Adelmann, J. Fink, J. T. Makert, M. B. Maple, S. Uchida, H. Takagi, Y. Tokura, A. C. W. P. James, and D. W. Murphy, Phys. Rev. B **43**, 333 (1991).

[7]N. Nüker, H. Romberg, X. X. Xi, and J. Fink, Phys. Rev. B **39**, 6619 (1989).

[8]H. Romberg, M. Alexander, N. Nücker, P. Adelmann, and J. Fink, Phys. Rev. B **42**, 8768 (1990).

[9]M. Matsuda, K. Yamada, K. Kakurai, H. Kadowaki, T. R. Thurston, Y. Endoh, Y. Hideka, R. J. Birgeneau, M. A. Kastner, P. M. Gehring, A. H. Moudden, and G. Shirane, Phys. Rev. B **42**, 10 098 (1990).

[10]R. J. Birgeneau and G. Shirane, in *Physical Properties of High-Temperature Superconductors I,* edited by D. M. Ginsberg (World Scientific, Singapore, 1989), p. 151.

[11]T. Chattopadhyay, P. J. Brown, B. Roessli, A. A. Stepanov, S. N. Barilo, and D. I. Zhigunov, Phys. Rev. B **46**, 5731 (1992).

[12]S. Skanthakumar, J. W. Lynn, J. L. Peng, and Z. Y. Li, J. Appl. Phys. **69**, 4866 (1991).

[13]I. Tomeno, M. Yoshida, K. Ikeda, K. Takamuku, N. Koshizuka, S. Tanka, K. Oka, and H. Unoki, Phys. Rev. B **43**, 3009 (1991).

[14]P. E. Sulewski, P. A. Fleury, K. B. Lyons, S.-W. Cheong, and Z. Fisk, Phys. Rev. B **41**, 225 (1990).

[15]T. Uzumaki, K. Hashimoto, and N. Kamehara, Physica C **202**, 175 (1992).

[16]P. E. Sulewski, P. A. Fleury, K. B. Lyons, and S.-W. Cheong, Phys. Rev. Lett. **67**, 3864 (1991).

[17]J. M. Tranquada, G. Shirane, B. Keimer, S. Shamoto, and M. Sato, Phys. Rev. B **40**, 4503 (1989).

[18]R. Liu, M. V. Klein, D. Salamon, S. L. Cooper, W. C. Lee, S.-W. Cheong, and D. M. Ginsberg, J. Phys. Chem. Solids **54**, 1347 (1993).

[19]M. V. Klein, R. Liu, D. Salamon, S. L. Cooper, W. C. Lee, D. M. Ginsberg, and S.-W. Cheong, J. Supercond. **7**, 429 (1994).

[20]D. Salamon, R. Liu, M. V. Klein, W. C. Lee, D. M. Ginsberg, and S.-W. Cheong (unpublished).

[21]R. Liu, D. Salamon, M. V. Klein, S. L. Cooper, W. C. Lee, S.-W. Cheong, and D. M. Ginsberg, Phys. Rev. Lett. **71**, 3709 (1993).

[22]D. R. Wake, Phys. Rev. B **49**, 3641 (1994).

[23]D. Salamon, Ran Liu, P. Abbamonte, M. V. Klein, I. I. Tartakovskii, W. C. Lee, D. M. Ginsberg, and B. W. Veal (unpublished).

[24]S. Uchida, T. Ido, H. Takagi, T. Arima, Y. Tokura, and S. Tajima, Phys. Rev. B **43**, 7942 (1991).

[25]Y. Tokura, S. Koshihara, T. Arima, H. Takagi, S. Ishibashi, T. Ido, and S. Uchida, Phys. Rev. B **41**, 11 657 (1990).

[26]K. Kubat-Martin, Z. Fisk, and R. R. Ryan, Acta Crystallogr. C **44**, 1518 (1988).

[27]S.-W. Cheong, J. D. Thompson, and Z. Fisk, Physica C **158**, 109 (1989).

[28]J. P. Rice, E. D. Bukowski, and D. M. Ginsberg, J. Low Temp. Phys. **77**, 119 (1989).

[29]J. P. Rice, B. G. Pazol, D. M. Ginsberg, T. J. Moran, and M. B. Weissman, J. Low Temp. Phys. **72**, 345 (1988).

[30]S. Jandl, M. Iliev, C. Thomsen, T. Ruf, M. Cardona, B. M. Wanklyn, and C. Chen, Solid State Commun. **87**, 609 (1993).

[31]S. Sugai, Phys. Rev. B **39**, 4306 (1989).

[32]E. T. Heyen, J. Kircher, and M. Cardona, Phys. Rev. B **45**, 3037 (1992).

[33]E. T. Heyen, R. Liu, M. Cardona, S. Piñol, R. J. Melville, D.

M. Paul, E. Morán, and M. A. Alario-Franco, Phys. Rev. B **43**, 2857 (1991).
[34]S. Sugai, T. Kobayashi, and J. Akimitsu, Solid State Commun. **74**, 599 (1990).
[35]P. Adelmann, R. Ahrens, G. Czjzek, G. Roth, H. Schmidt, and C. Steinleitner, Phys. Rev. B **46**, 3619 (1992).
[36]M. A. Laguna, M. L. Sanjuán, A. Butera, M. Tovar, Z. Fisk, and P. Canfield, Phys. Rev. B **48**, 7565 (1993).
[37]M. Udagawa, Y. Nagaoka, N. Ogita, M. Masada, J. Akimitsu, and K. Ohbayashi, Phys. Rev. B **49**, 585 (1994).
[38]S. B. Oseroff, D. Rao, F. Wright, D. C. Vier, S. Schultz, J. D. Thompson, Z. Fisk, S.-W. Cheong, M. F. Hundley, and M. Tovar, Phys. Rev. B **41**, 1934 (1990).
[39]A. A. Stepanov, P. Wyder, T. Chattopadhyay, P. J. Brown, G. Fillion, I. M. Vitebsky, A. Deville, B. Gaillard, S. N. Barilo, and D. I. Zhigunov, Phys. Rev. B **48**, 12 979 (1993).
[40]I. M. Vitebskii and A. A. Stepanov, Fiz. Nizk. Temp. **19**, 226 (1993) [Low Temp. Phys. **19**, 160 (1993)].
[41]R. D. Zysler, M. Tovar, C. Rettori, D. Rao, H. Shore, S. B. Oseroff, D.C. Vier, S. Schultz, Z. Fisk, and S.-W.Cheong, Phys. Rev. B **44**, 9467 (1991).
[42]V. N. Denisov, C. Taliani, A. G. Mal'shukov, V. M. Burlakov, E. Schönherrr, and G. Ruani, Phys. Rev. B **48**, 16 714 (1993).
[43]M. J. Akhtar, C. R. A. Catlow, S. M. Clark, and W. M. Temmerman, J. Phys. C **21**, L917 (1988).
[44]M. C. Aronson, S. B. Dierker, B. S. Dennis, S.-W. Cheong, and Z. Fisk, Phys. Rev. B **44**, 4657 (1991).
[45]M. I. Eremets, A. V. Lomsadze, V. V. Struzhkin, A. A. Maksimov, A. V. Puchkov, and I. I. Tartakovskii, JETP Lett. **54**, 372 (1991).
[46]A. A. Maksimov and I. I. Tartakovskii, J. Supercond. **7**, 439 (1994).
[47]J. Gopalakrishnan, M. A. Subramanian, C. C. Torardi, J. P. Attfield, and A. W. Sleight, Mater. Res. Bull. **24**, 321 (1989).
[48]D. E. Cox, A. I. Goldman, M. A. Subramanian, J. Gopalakrishnan, and A. W. Sleight, Phys. Rev. B **40**, 6998 (1989).
[49]R. M. Hazen, in *Physical Properties of High-Temperature Superconductors II,* edited by D. M. Ginsberg (World Scientific, Singapore, 1990), p. 121.
[50]D. V. Khveshchenko and P. B. Wiegmann, Phys. Rev. Lett. **73**, 500 (1994).
[51]R. L. Martin and P. J. Hay, J. Chem. Phys. **98**, 8680 (1993).
[52]J. F. Annett, R. M. Martin, A. K. McMahan, and S. Satpathy, Phys. Rev. B **40**, 2620 (1989).
[53]A. K. McMahan, R. M. Martin, and S. Satpathy, Phys. Rev. B **38**, 6650 (1988).
[54]J. P. Falck, J. D. Perkins, A. Levy, M. A. Kastner, J. M. Graybeal, and R. J. Birgeneau, Phys. Rev. B **49**, 6246 (1994).
[55]J. D. Perkins, J. M. Graybeal, M. A. Kastner, R. J. Birgeneau, J. P. Falck, and M. Greven, Phys. Rev. Lett. **71**, 1621 (1993).
[56]G. Yu, C. H. Lee, D. Mihailovic, and A. J. Heeger, Phys. Rev. B **48**, 7545 (1993).
[57]R. R. P. Singh, P. A. Fleury, K. B. Lyons, and P. E. Sulewski, Phys. Rev. Lett. **62**, 2736 (1989).
[58]S. Tajima, T. Ido, S. Ishibashi, T. Itoh, H. Eisaki, Y. Mizuo, T. Arima, H. Takagi, and S. Uchida, Phys. Rev. B **43**, 10 496 (1991).
[59]J. B. Grant and A. K. McMahan, Phys. Rev. B **46**, 8440 (1992).